Physics of the Earth and Planetary Interiors 242 (2015) 1–8

Contents lists available at ScienceDirect

Physics of the Earth and Planetary Interiors

journal homepage: www.elsevier.com/locate/pepi

On the role of thermal heterogeneities on the rheology of MgO under conditions of the Earth's lower mantle

J. Amodeo [a,b,*], B.S.A. Schuberth [c], H.-P. Bunge [c], Ph. Carrez [b], P. Cordier [b]

[a] Laboratoire MATEIS CNRS UMR 5510, Université de Lyon, INSA-Lyon, F-69621 Villeurbanne Cedex, France
[b] Unité Matériaux et Transformation CNRS UMR 8207, Université de Lille 1, Bat C6, F-59655 Villeneuve D'Ascq, France
[c] Geophysics Section – Dept. of Earth and Environmental Sciences, Ludwig-Maximilians-Universität München, Theresienstr. 41, 80333 München, Germany

ARTICLE INFO

Article history:
Received 30 September 2014
Received in revised form 11 February 2015
Accepted 24 February 2015
Available online 3 March 2015

Keywords:
Multiscale modelling
Geodynamics
Dislocation
Lower mantle rheology

ABSTRACT

The Earth's mantle is characterised by large thermal heterogeneities associated with hot rising plumes and cold downwelling slabs. These lateral temperature variations in excess of 1000 K may have a crucial influence on the rheology of mantle rocks. Here we use a numerical multiscale model that allows us to make predictions from first principles with no adjustable parameters on the deformation of MgO under the extreme conditions of mantle pressure, temperature and strain rate, in order to investigate the sensitivity of mantle viscosity to the temperature heterogeneities inferred from a global high resolution mantle circulation model. Our results show that under the very low strain rates of the mantle, MgO deforms mostly at low stresses (few tens of MPa) in an athermal regime, where the deformation is insensitive to both temperature and strain rate, leading to a very weak phase throughout much of the upper half of the lower mantle. In its lower half, the weak phase gives way to high material strength with thermally activated viscosities in the cold downwelling slabs, while much of the hot upwelling flow remains in the athermal regime, resulting in large lateral variations in the inferred material strength of MgO. Our results suggest the presence of large lateral viscosity variations in the deepest parts of the lower mantle, associated in particular with the graveyard of old subducted oceanic lithosphere.

1. Introduction

Much of the geological activity (plate tectonics, volcanism or mountain building) observed at the surface of our planet is driven by convection in Earth's mantle. Being mostly constituted of solid rocks, its flow results from the ability of mantle minerals and polycrystalline assemblages to creep under very slow strain rates. The extreme pressure and temperature conditions of the Earth's mantle have profound implications on the rheology of rocks and minerals. In recent years considerable efforts have been devoted to the development of deformation experiments under mantle *P*, *T* conditions. However, most of the mantle remains inaccessible to experimental studies of deformation. Multiscale modelling represents a promising alternative to describe the behaviour of solids. It allows one to link our understanding of a few elementary mechanisms (usually at the microscopic scale) with the behaviour observed at the macroscopic scale. This approach has been recently applied to model plastic flow in MgO under Earth's mantle pressure, temperature and strain rates (Cordier et al., 2012). We found that once the influence of pressure and strain rate are taken into account, the rheology of MgO strongly depends on temperature. Above a critical temperature T_a called the athermal transition temperature, thermal activation is sufficient to overcome lattice friction and incipient plastic shear becomes temperature independent. The solid exhibits a purely plastic behaviour and flows under a constant stress determined by the microstructure. Below T_a, the rheology of MgO is thermally activated and can be described through a viscous flow law. Comparing T_a with mantle temperatures puts strong constraints on the rheology of MgO. In Cordier et al. (2012), T_a has been compared with the average temperature increase through the Earth's mantle (the geotherm). The temperature of the geotherm rises only slightly with depth throughout most of the mantle. Only in the narrow thermal boundary layer at the core mantle boundary does the temperature increase rapidly over a depth range of a few hundred kilometres. This has led to a layered model where the viscous rheology of MgO would be restricted to a c.a. 500 km-thick layer at the base of the lower mantle. Although the lower mantle has long been supposed to have rather simple properties, which could be described within a radial 1D model, there is

* Corresponding author at: Laboratoire MATEIS – UMR CNRS 5510, Groupe METAL, Groupe CERA, 25 avenue Jean Capelle, Bat. St. Exupéry, 2ème étage, 69621 Villeurbanne Cedex, France. Tel.: +33 04 72 43 82 35; fax: +33 04 72 43 85 39.
E-mail address: jonathan.amodeo@insa-lyon.fr (J. Amodeo).

http://dx.doi.org/10.1016/j.pepi.2015.02.008
0031-9201/

increasing evidence for a range of complexity, which calls for a description of 3D heterogeneities. Recent high-resolution global mantle circulation models (MCMs) have highlighted the importance of thermal heterogeneities, which can be of the order of ±1000 K. In the present study, we take advantage of the results of such MCM to describe the spatial variations of the rheological properties of MgO under lower mantle conditions.

2. Multiscale modelling of the rheology of MgO under lower mantle conditions

Here we briefly present the multiscale model of MgO deformation developed in Amodeo et al. (2011) and recently applied at Earth's lower mantle conditions (Cordier et al., 2012). Plastic deformation of solids is carried by lattice defects (point defects, dislocations, grain boundaries). Dislocations represent generally the most efficient strain-producing mechanism, so we focused on the contribution of dislocation glide on the rheology of MgO. Indeed we observe in most materials that lattice friction (i.e. the force opposed to dislocation motion) increases under the influence of confining pressure (Bulatov et al., 1999; Carrez et al., 2009; Yang et al., 2001). The ability of dislocations to glide and produce strain under mantle conditions is thus a fundamental parameter. Lattice friction results from the actual atomic arrangements on the dislocation line, a region called the dislocation core. The more a dislocation core spreads into a given crystallographic plane, the easier is its glide in this plane. In MgO, there exist only one kind of dislocations characterised by their Burgers vector $\frac{1}{2}\langle 1\,1\,0\rangle$ (i.e., the elementary shear left after the dislocation line) which can glide in several potential crystallographic planes, {1 0 0} and {1 1 0} being the most common. In this approach, the core structure of $\frac{1}{2}\langle 1\,1\,0\rangle$ dislocations is modelled using the Peierls–Nabarro–Galerkin method (Denoual, 2004) with γ-surfaces calculated at the atomic scale from first-principles as an input. This is where the electronic structure and the influence of pressure are taken into account. We find that under increasing confining pressure over c.a. 30 GPa, the easiest slip planes switch from {1 1 0} to {1 0 0} (Amodeo et al., 2012). This property has been confirmed by deformation-DIA creep experiments (Girard et al., 2012). Dislocation motion under finite temperature results from the conjugate influence of stress and thermal activation. The glide mechanism involves nucleation of kink pairs on the dislocation line, which represents the critical configuration between two dislocation positions. The activation enthalpies for this kink-pair mechanism are determined using the elastic interaction method (Koizumi et al., 1993). This knowledge allows one to derive flow stress profiles $\sigma(P, T)$ (i.e., the critical stress required to plastically deform MgO) from mesoscopic scale approaches such as discrete dislocation dynamics simulations (Bulatov et al., 2006; Devincre and Kubin, 1997; Weygand and Gumbsch, 2005). Our results show that deformation mechanisms are highly temperature-dependent in MgO. However, two regimes must be distinguished. Based on the terminology used for metallic materials (Kubin et al., 1998), we define two main deformation regimes delimiting the athermal transition temperature T_a. The two regimes account for different mechanisms resulting in contrasted macroscopic behaviours:

(i) the *thermally activated regime* which is effective below T_a accounts for lattice friction on individual dislocations. There, dislocation-produced flow is time dependent and results in an apparent viscosity.
(ii) the *athermal regime* where the dislocation microstructure and contact reactions between defects govern plasticity. There, dislocation-produced flow is time independent and MgO behaves as a pure plastic solid. Even if an apparent viscosity can always be calculated from the ratio of the stress to the strain-rate, its value is non uniquely defined since the stress is not any more controlled by the strain-rate, but by an uncontrolled, external, parameter: the dislocation microstructure.

Table 1 shows $v(P, T)$ viscosity profile for $10^{-16}\,s^{-1}$ imposed strain rate and low dislocation density ($10^8\,m^{-2}$). At low temperatures, deep in the thermally activated regime, dislocation glide is controlled by lattice friction that constrains deformation under high stresses only. This is where rheology becomes highly non-linear and viscosity reaches values up to 10^{24}–10^{25} Pa s. For close-to-T_a temperatures, stresses decrease due to the temperature contribution to the activation energy. This leads to lower viscosity values nearby the 10^{21}–10^{22} Pa s range expected for the Earth's mantle viscosity (Mitrovica and Forte, 2004). In Table 1, blanks stand for temperatures above T_a (athermal regime) where stresses are governed by the forest dislocations microstructure (Amodeo et al., 2014) and do not depend on strain rate. Therefore, the model does not enable univocal viscosity calculation for this regime. In order to fit the thermal heterogeneity model, data presented in Table 1 have been interpolated every 10 K/0.5 GPa using splines. In the mantle conditions of strain rate, the computed viscosity profile is not sensitive to dislocation density (see Supplementary information at for further details on this issue). The viscosity map $v(P, T)$ is presented Fig. 1.

3. Temperature field from a mantle circulation model

Mantle circulation models have now reached a state where they are able to represent a realistic range of temperature variations in the Earth's mantle (Bower et al., 2013; Davies et al., 2012; Schuberth et al., 2009b). This is achieved through numerically solving the set of equations that govern the motion of a viscous fluid at sufficiently high grid point resolution to model flow at Earth-like convective vigour; that is, at Rayleigh numbers of the order of

Table 1
Multiscale viscosity model of MgO calculated for $10^{-16}\,s^{-1}$ strain rate. Values are in Pa s.

Temperature (K)	Pressure (GPa)			
	30	60	100	140
0	6.00E+24	7.50E+24	9.20E+24	1.15E+25
100	4.60E+24	6.26E+24	8.42E+24	1.06E+25
200	3.56E+24	5.12E+24	7.64E+24	9.65E+24
300	2.71E+24	4.50E+24	6.89E+24	8.78E+24
400	1.99E+24	3.93E+24	6.17E+24	7.96E+24
500	1.41E+24	3.40E+24	5.48E+24	7.17E+24
600	9.37E+23	2.91E+24	4.83E+24	6.43E+24
700	5.73E+23	2.46E+24	4.22E+24	5.74E+24
800	3.08E+23	2.05E+24	3.66E+24	5.08E+24
900	1.34E+23	1.68E+24	3.13E+24	4.47E+24
1000	4.03E+22	1.34E+24	2.65E+24	3.90E+24
1100	6.43E+21	1.05E+24	2.21E+24	3.37E+24
1200	5.09E+20	8.00E+23	1.81E+24	2.89E+24
1300		5.86E+23	1.45E+24	2.44E+24
1400		4.10E+23	1.14E+24	2.04E+24
1500		1.29E+23	8.70E+23	1.68E+24
1600		4.30E+22	6.41E+23	1.36E+24
1700		1.02E+22	4.52E+23	1.07E+24
1800		1.79E+21	3.02E+23	8.30E+23
1900			1.87E+23	6.22E+23
2000			1.06E+23	4.50E+23
2100			5.31E+22	3.12E+23
2200			1.98E+22	2.04E+23
2300			5.66E+21	1.25E+23
2400			1.44E+21	6.96E+22
2500				3.50E+22
2600				1.55E+22
2700				6.07E+21
2800				2.14E+21

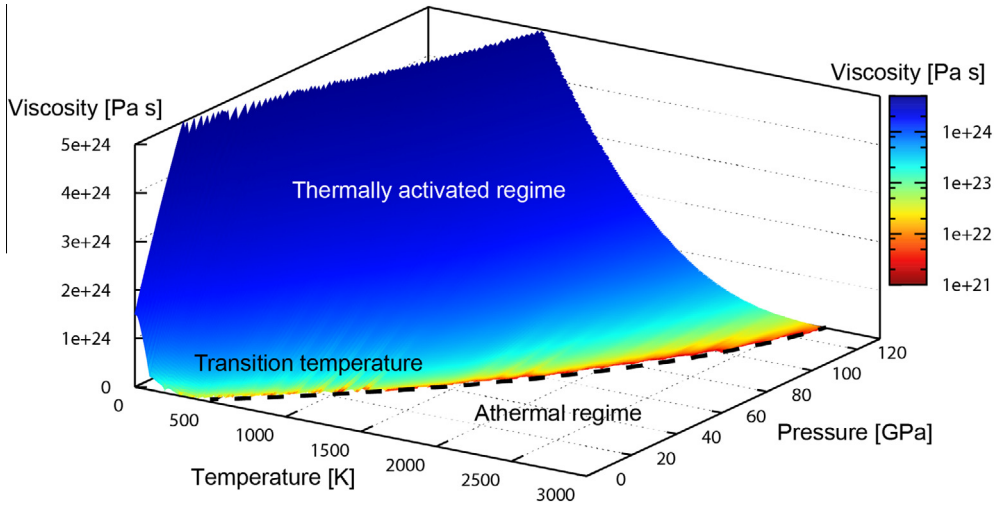

Fig. 1. Interpolated $v(P,T)$ viscosity profile for 10^{-16} s^{-1} strain rate. The dashed line refers to the athermal transition temperature.

10^8–10^9. Here we use the mantle circulation model M2 of (Schuberth et al., 2009b), which will be called S09-M2 in the following. The calculations were done with the parallel finite element code TERRA (Bunge et al., 1996, 1997) that was implemented on a dedicated compute cluster designed for large-scale geophysical modelling (Oeser et al., 2006). TERRA solves for the momentum and energy balance at infinite Prandtl number (i.e. no inertial forces) in a spherical shell. Compressibility effects are incorporated in form of the anelastic liquid approximation. The effects of phase transitions on mantle flow dynamics are not included in model S09-M2.

Apart from a high numerical resolution with global grid spacing of c.a. 25 km, model S09-M2 is based on a minimum set of assumptions: (1) a large-scale flow structure related to the history of plate motions (Lithgow Bertelloni and Richards, 1998; Ricard et al., 1993), which is assimilated into the model as time-dependent surface velocity boundary conditions, (2) a radial three-layer viscosity profile that agrees with post-glacial rebound and geoid observations (Hager, 1984; Paulson et al., 2007) as well as with the inferred rate of true polar wander (Schaber et al., 2009). The three layers are identified as the lithosphere, upper mantle and lower mantle, separated at 100 and 650 km depth with assigned viscosities of 10^{23}, 10^{21} and 10^{23} Pas respectively, (3) isochemical whole mantle flow with strong plume flux (Bunge, 2005). To this end, the CMB temperature is kept constant at 4200 K, which yields a core heat flow or c.a. 12 TW (about 35% of the outflow at the top of the mantle).

Most important to note here is that the temperature variations of S09-M2, give rise to seismic heterogeneity that compares well to tomographic models of shear wave velocity in terms of the magnitude of anomalies (Schuberth et al., 2009a). Furthermore, long-period body wave traveltime residuals obtained from simulations of wave propagation through the synthetic seismic structures of S09-M2 match the seismic observations well in terms of their standard deviation (Schuberth et al., 2012).

Fig. 2 (left panel) shows the range of temperatures in the mantle predicted from model S09-M2. Plotted are the global minimum, mean, and maximum temperatures as a function of depth. In a vigorously convecting and well-mixed mantle, the temperature distribution is typically characterised by a large peak close to the mean in most depths (i.e. much of the mantle volume comprises regions having temperatures close to mean temperature of that depth level) away from the thermal boundary layers. Weak and extended tails on either side of the peak correspond to the sinking

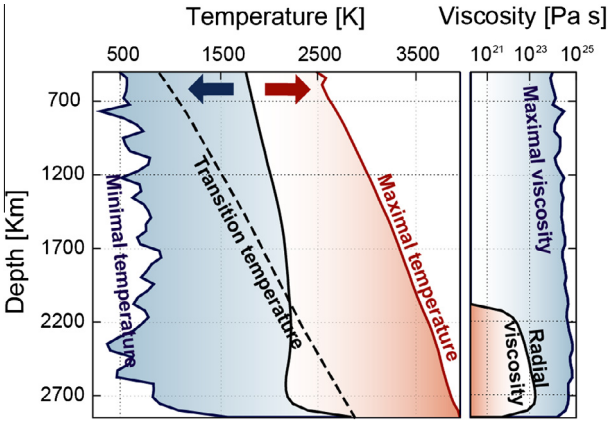

Fig. 2. Temperature and viscosity extrema. On the left panel, solid lines represent the global mean temperature (black) in addition to negative (blue) and positive (red) larger lateral temperature variations inferred from the S09-M2 model (Schuberth et al., 2009b). The dashed line shows the athermal transition temperature T_a deduced from the multiscale model of MgO deformation (Amodeo et al., 2011; Cordier et al., 2012). On the right panel, the solid black line circles a viscosity window (radial viscosity) referring to the global mean temperature. The solid blue line refers to higher viscosity values, deduced from the larger negative variations of temperature. (For interpretation of the references to colour in this figure legend, the reader is referred to the web version of this article.)

slabs on the cold and active upwelling plumes on the hot side. The temperature decrease of hot upwellings during their ascent through the mantle is much larger than the temperature increase of the downgoing slabs. This depth-dependence of both cold and hot temperatures seen in Fig. 2 and the related negative and positive excess temperatures (i.e., difference with respect to the mean) can be understood from the combination of two effects: (i) The adiabatic gradient in the mantle depends on temperature and is thus different for different potential temperatures (i.e., cold and hot mantle material); (ii) The mean mantle geotherm likely is sub-adiabatic due to internal heating by radioactive decay (e.g., Bunge, 2005).

For the cold slab material in the mantle, which has low potential temperatures, this means that the adiabatic temperature increase is modest. In addition, thermal conduction is not effective enough to heat the material during its descent in the mantle. Thus, temperatures in the coldest regions increase only slightly from

around 500 K at the top of the lower mantle to roughly 800–900 K close to the core-mantle boundary (CMB). The variability of the minimum temperature with depth is related to the fact that plate motion histories are used as surface boundary condition. This leads to a varying amount of cold material over time that enters the material during subduction. Moreover, the descending material corresponds to plates of different age, which therefore will have different slab temperatures.

Hot upwellings in model S09-M2 are generated from the strong thermal boundary layer in D″ that develops due to the CMB temperature boundary condition of 4200 K. This CMB temperature is in agreement with a large number of recent studies, as discussed in Schuberth et al. (2009b), and gives rise to plume excess temperatures in the lowermost mantle of around +1000 K and more. Near the surface, however, excess temperatures of mantle upwellings as obtained from petrological measurements are rather small, ranging between +200 and +300 K (e.g., Schilling, 1991). Nevertheless, these numbers are entirely consistent with a high CMB temperature and a strong thermal gradient across the D″. The maximum absolute temperatures in the mantle decrease strongly from bottom to top. Plumes experience a strong temperature reduction during their ascent, as they follow a steeper adiabatic gradient compared to the slabs owing to their higher potential temperature. The temperature distribution in plumes is expected to be nearly adiabatic, as they rise relatively quickly through the mantle, on a timescale on the order of a few tens of Myrs. In combination with the sub-adiabaticity of the ambient mantle, this leads to the large differences in excess temperatures between deep and shallow mantle mentioned above.

4. Implications of thermal heterogeneities on the rheology of MgO

4.1. Radial distribution

Cordier et al. (2012) show that viscosity may be deduced from flow stress profiles $\sigma(P, T)$ below T_a. In the case where a simple radial temperature profile is considered, only the deepest part of the mantle (beyond 2000 km depth) is characterised by the thermally activated regime of MgO and thus shows a viscosity in the range of 10^{21}–10^{22} Pa s (referred as *radial viscosity* in Fig. 2).

Based on a simple bracketing algorithm, the multiscale viscosity model is constrained for the coldest temperatures of model S09-M2 (Fig. 2, blue curve), which are well below the mean temperature. For this purpose, the pressure/depth relation is described by a fourth order polynomial adjustment of the PREM model (Dziewonski and Anderson, 1981). Results are presented Fig. 2, right panel.

In case of the large negative temperature variations, the window in which viscosity can be defined (*maximal viscosity* in Fig. 2) is now considerably enlarged covering the entire lower mantle compared to the one deduced from the mean temperature profile (*radial viscosity* in Fig. 2). Furthermore, as emphasised in Table 1, viscosity increases with decreasing temperature. In addition to its spatial range, the viscosity amplitude is therefore also raised up to 10^{24}–10^{25} Pa s for the coldest temperatures, which coincide with maximal lattice friction. The inferred average radial viscosity values for the deepest part of the lower mantle are around 10^{23} Pa s. It is important to note that this is the same as used in the underlying mantle circulation model and variations around that value stay below 1 to 2 orders of magnitude throughout the entire lower mantle.

An interesting observation is that below a depth of about 2100–2200 km, also material warmer than average is in the thermally activated regime. In other words, in the lowermost few hundred kilometres of the mantle, it is possible to apply the multiscale viscosity model also for part of the upwelling plume material, which has moderate excess temperatures. The dashed line in Fig. 2, in fact, shows that the closer the material is to the CMB, the hotter the material can get to still be in the thermally activated regime. This is intriguing as it may have consequences on the dynamics of the lowermost mantle, in particular at the edges of upwelling regions; that is, at the contact between accumulated slabs and the large low shear velocity provinces (LLSVP) imaged by seismic tomography (e.g., Grand et al., 1997; Houser et al., 2008; Kennett et al., 1998; Kustowski et al., 2008; Li et al., 2008; Masters et al., 2000; Montelli et al., 2006; Panning and Romanowicz, 2006; Ritsema et al., 2010; Simmons et al., 2010; van der Hilst et al., 1997). Most important, the depth range in which part of the buoyant material can be assigned a viscosity by the rheological model is limited to the lowermost ~500 km of the mantle, which coincides with the height of the seismically imaged LLSPVs. Below, we discuss the lateral variations in viscosity that result from the temperature distribution of model S09-M2 in more detail to illustrate where the potential dynamical consequences could be most relevant. We note that in this study we focus on describing the viscosity variations that result from post-processing of the temperature field of the mantle circulation model with the multiscale approach of MgO deformation. We do not provide a full numerical investigation of the dynamic consequences of the rheological model and its feedback on mantle flow. This would require modelling the mechanical properties of other rock phases as olivine and perovskites, which is postponed to a future study.

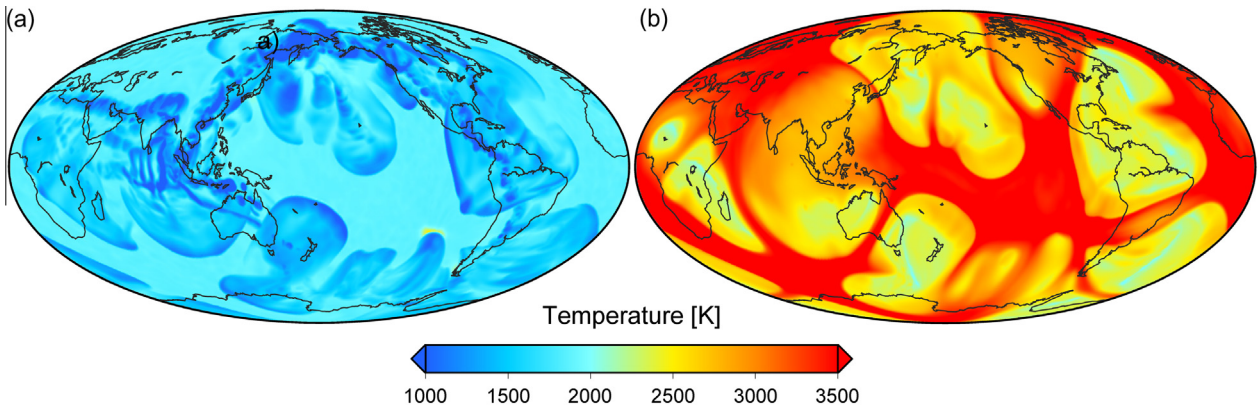

Fig. 3. Extreme values of temperature below each point of latitude and longitude in model S09-M2. Left: the minimum temperature; right: the maximum temperature.

4.2. Lateral variations

Fig. 3 shows how the extreme values of temperature in model S09-M2 vary spatially. Plotted is the minimum temperature below each point of latitude and longitude (left panel) as well as the maximum temperature (right panel). One can see that minimum and maximum temperature regions exhibit a high radial correlation; that is, higher temperatures on the map of minima relate to higher temperatures on the map of maxima (and vice versa). In other words, cold and hot regions are underlain by cold and hot

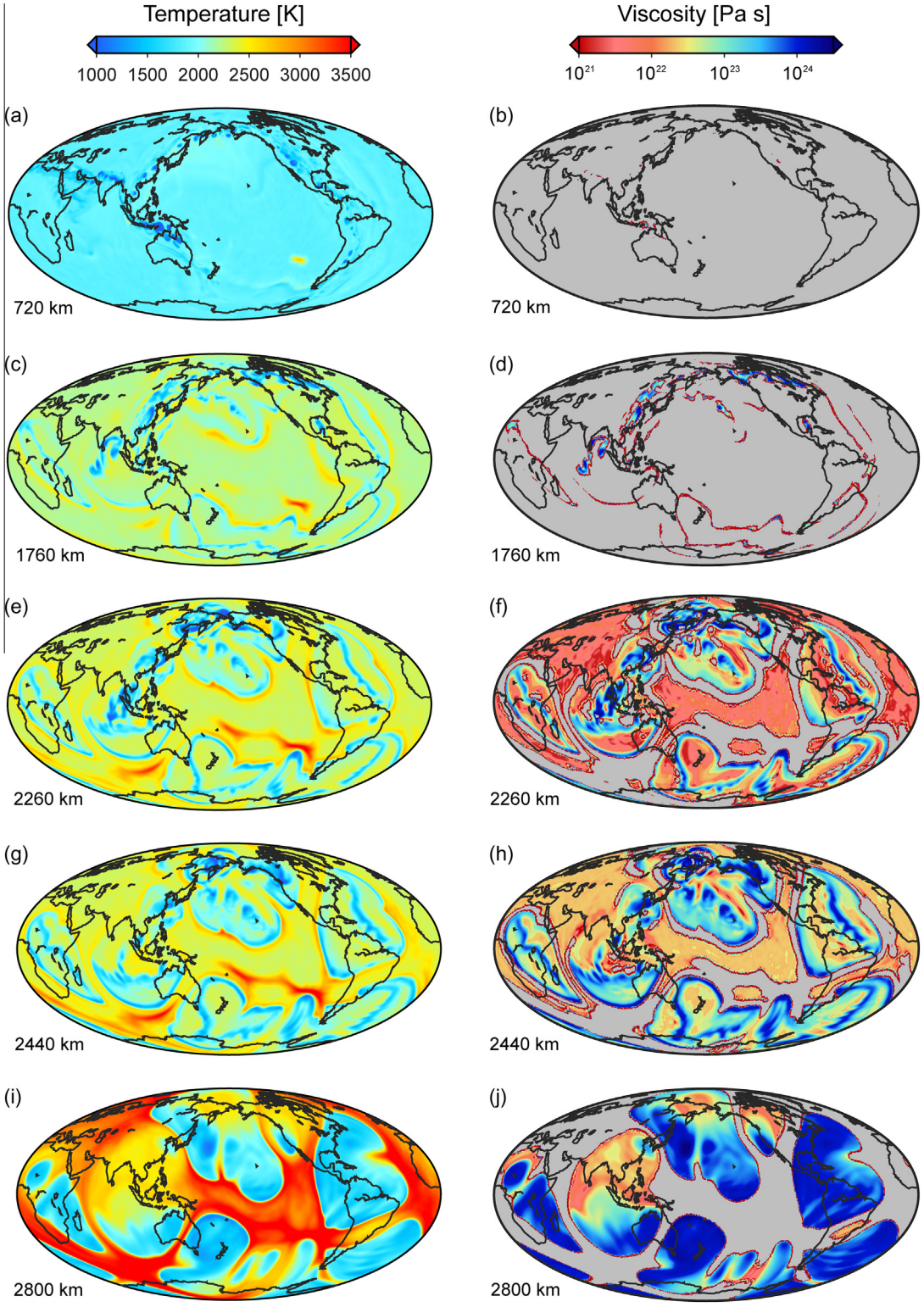

Fig. 4. Temperature and viscosity variations at 720, 1760, 2260, 2440 and 2800 km depth. Grey domains refer to athermal regime conditions where viscosity cannot be inferred from the multiscale viscosity model.

material also at greater depths, respectively. Such vertical coherence is characteristic for buoyancy driven convection and is also imaged by seismic tomography for Earth's mantle (e.g., Becker and Boschi, 2002). This behaviour can, for example, be seen for the circum-Pacific region that has experienced subduction over the past 200 Ma (e.g., Seton et al., 2012). Inside the Earth's lower mantle, it is thus possible to distinguish cold regions (e.g., below the Cocos, the Caribbean and parts of the North-American plates as well as below the south and eastern part of the Eurasian plate) and warm regions (e.g., below the centre of the Pacific plate and between Africa and the Mid-Atlantic ridge down to the Southwest Indian ridge as well as below the centre of Eurasia), where the colder regions have been referred to as a graveyard for subducted oceanic lithosphere (e.g., Richards and Engebretson, 1992).

The temperature distribution inside Earth's lower mantle as given by model S09-M2 has a strong impact on the lateral variations in viscosity. Fig. 4 shows the predicted viscosity distribution at depths of 720, 1760, 2260, 2440 and 2800 km. See Supplementary materials at for videos which detail the evolution of temperature and viscosity profiles throughout the entire lower mantle. While viscosity can be defined only in very few regions of the upper part of the lower mantle (i.e., at 720 km depth, Fig. 4a and b), larger domains occur deeper. At 1760 km depth (Fig. 4c and d), several low temperature regions exist where viscosity domains already appear, for example below the south of the Eurasian plate and the upper part of the North-American plate. These regions correspond to material of the subducted Pacific and Farallon plates, respectively.

Boundaries defined by locally higher temperatures surround such domains, which appear as a pattern of alternating low and high temperatures underlined by blue and red linear features, respectively. The higher temperatures in these boundary regions do not lead to domains where viscosity can be defined (i.e., they are too hot to be in the thermally activated regime), while cooler regions exist right next to them for which the rheological model predicts rather low viscosities of around 10^{20}–10^{21} Pa s.

The elevated temperatures around cold material are related to the fact that slabs reaching the CMB need to spread horizontally thereby pushing hot material upward. This hot upwelling material itself drags part of the cold slab material upward again by viscous coupling, which gives rise to moderately cold temperature streaks paralleling the hot linear features.

In the deepest part of the lower mantle below 2000 km depth, viscosity domains can be clearly identified in Fig. 4f, h and j that correlate well with the low-temperature domains of Fig. 4e, g and i. Corresponding viscosities range between 10^{22} and 10^{24} Pa s with a strong dominance towards higher values so that most of the cold regions directly above the CMB are mechanically rather strong. Most of the warm areas, on the other hand, are in the athermal regime, as can be seen from the large grey regions in the viscosity map at 2800 km depth (Fig. 4j). The dynamically most interesting effect at that depth appears at the borders of the hot regions. There, temperatures, while being higher than average, are low enough to fall within the thermally activated regime. Therefore, viscosities can be defined, which however, are rather low with values of less than 10^{21} Pa s. As can be seen from Fig. 4j, these regions of moderately hot and low viscosity material encircle the hot upwelling regions as very thin bands. These weak bands could potentially represent regions of localised deformation decoupling to some extent the upwelling material from the surrounding mantle. The dynamic consequences, however, are difficult to predict, as the major part of the upwellings is predominantly in the athermal regime; that is, dominated by plastic instead of viscous flow.

Further interesting effects of the temperature variations in model S09-M2 on the distribution of viscosity happen at 2260 and 2440 km depth. There, the slabs also show very high viscosities of 10^{24} Pa s; that is, similar to the values of the cold spread-out regions right above the CMB. Most of the edges of the hot regions are still in the athermal regime, as well as some very hot parts in their interior. However, at these shallower depths vast parts are cool enough to show viscosities, for example, in the centre of the Pacific, under most of Eurasia, and under South Africa and the eastern part of the Atlantic. At 2440 km depth, the viscosities in these warm regions are on the order of 5×10^{22} Pa s, while they are only around $1–5 \times 10^{21}$ Pa s further up at 2260 km depth. Interesting to note is that the boundary regions of upwellings are to a large extent in the athermal regime, which on the warm side (i.e., towards their interior) are bounded by very low viscosities of less than 10^{21} Pa s. At the contact to the cold regions, viscosities first are very low, also at less than 10^{21} Pa s, which however then pass through into very high values of around 10^{24} Pa s for regions with the coldest temperatures before falling off to lower values again for the moderately cold regions further away from the hot areas. The potential importance of this complex behaviour becomes clear in the light of direct seismic observations made at the rims of the LLSVPS, which seem to be characterised by steep edges with sharp gradients in seismic velocities (e.g., To et al., 2005).

5. Concluding remarks

The primary goal of our work is to link our understanding of deformation mechanisms at the microscopic scale with the behaviour observed at the macroscopic scale, thereby improving our insight into the different rheological regimes that may exist under the extreme pressure and temperature conditions of the deep Earth. Since much of the mantle remains inaccessible to experimental studies of deformation, not least because of the low strain rates prevailing under the conditions of the solid-state convective motion of the mantle, multiscale material deformation modelling offers much potential to constrain deep mantle flow regimes.

An important result, also reported in Cordier et al. (2012), is the occurrence of an athermal regime of MgO throughout much of the upper part of the lower mantle. In this mantle region, MgO seems to be weak and a viscosity cannot be defined. In fact, geodynamicists have known for a long time that mantle flow models using a simple, linear, depth-dependent rheology provide a good fit to the observed long-wavelength Geoid (e.g., Hager and Richards, 1989). Our predictions from the rheological model of MgO seem to be consistent with this result. Deformation in the upper part of the lower mantle is only mildly dependent on strain rate in the regions that are cold enough to be in the thermally activated regime (at these depths, stress exponents are close to 1 for relevant temperatures; c.f. Fig. 3 in (Cordier et al., 2012)). The vast majority of the lower mantle upper part, however, is in the athermal regime, where deformation is also insensitive to temperature in addition to being insensitive to strain rate. At greater depth, the viscosity increases again due to the increasing influence of pressure. Equally interesting is the possibility, suggested by our modelling results, that large viscosity variations may be associated with the strong lateral temperature variations expected in the deep mantle. In particular, we find that high material strength may be linked to the low temperature of subducting oceanic slabs. The possibility of significant mechanical strength residing within subducted oceanic lithosphere agrees with the low sinking rates (on the order of 1 cm/yr) inferred from seismic tomographic models for downgoing oceanic slabs (e.g., Butterworth et al., 2014; Ricard et al., 1993; Shephard et al., 2012).

Acknowledgements

This work was partly supported by funding from the European Research Council under the Seventh Framework Programme (FP7), ERC grant N° 290424 – RheoMan to Patrick Cordier. The dedicated compute cluster at LMU Munich was funded through the HBFG program (grant 132-943-1) of the German Science Foundation. The simulations used in this study were partly computed on the supercomputing facilities of the Leibniz-Rechenzentrum (LRZ) Munich, Germany. We thank the staff of the LRZ for their support.

Appendix A. Supplementary data

Supplementary data associated with this article can be found, in the online version, at http://dx.doi.org/10.1016/j.pepi.2015.02.008.

References

Amodeo, J., Carrez, P., Cordier, P., 2012. Modelling the effect of pressure on the critical shear stress of MgO single crystals. Philos. Mag. A 92, 1523–1541. http://dx.doi.org/10.1080/14786435.2011.652689.

Amodeo, J., Carrez, P., Devincre, B., Cordier, P., 2011. Multiscale modelling of MgO plasticity. Acta Mater. 59, 2291–2301. http://dx.doi.org/10.1016/j.actamat.2010.12.020.

Amodeo, J., Devincre, B., Carrez, P., Cordier, P., 2014. Dislocation reactions, plastic anisotropy and forest strengthening in MgO at high temperature. Mech. Mater. 71, 62–73. http://dx.doi.org/10.1016/j.mechmat.2014.01.001.

Becker, T.W., Boschi, L., 2002. A comparison of tomographic and geodynamic mantle models. In: Geochem. Geophys. Geosyst. 3. http://dx.doi.org/10.1029/2001GC000168, −n/a.

Bower, D.J., Gurnis, M., Seton, M., 2013. Lower mantle structure from paleogeographically constrained dynamic Earth models. Geochem. Geophys. Geosyst. 14, 44–63. http://dx.doi.org/10.1029/2012GC004267.

Bulatov, V., Hsiung, L., Tang, M., Arsenlis, A., Bartelt, M., Cai, W., Florando, J., Hiratani, M., Rhee, M., Hommes, G., 2006. Dislocation multi-junctions and strain hardening. Nature 440, 1174–1178. http://dx.doi.org/10.1038/nature04658.

Bulatov, V., Richmond, O., Glazov, M., 1999. An atomistic dislocation mechanism of pressure-dependent plastic flow in aluminum. Acta Mater. 47, 3507–3514. http://dx.doi.org/10.1016/S1359-6454(99)00154-8.

Bunge, H., 2005. Low plume excess temperature and high core heat flux inferred from non-adiabatic geotherms in internally heated mantle circulation models. Phys. Earth Planet. Int. 153, 3–10. http://dx.doi.org/10.1016/j.pepi.2005.03.017.

Bunge, H.P., Richards, M.A., Baumgardner, J.R., 1996. Effect of depth-dependent viscosity on the planform of mantle convection. Nature 379, 436–438.

Bunge, H.P., Richards, M.A., Baumgardner, J.R., 1997. A sensitivity study of three-dimensional spherical mantle convection at 10exp8 Rayleigh number: effects of depth-dependent viscosity, heating mode, and an endothermic phase change. J. Geophys. Res. Solid Earth 102, 11991–12007. http://dx.doi.org/10.1029/96JB03806.

Butterworth, N.P., Talsrna, A.S., Mueller, R.D., Seton, M., Bunge, H.P., Schuberth, B.S.A., Shephard, G.E., Heine, C., 2014. Geological, tomographic, kinematic and geodynamic constraints on the dynamics of sinking slabs. J. Geodyn. 73, 1–13. http://dx.doi.org/10.1016/j.jog.2013.10.006.

Carrez, P., Ferré, D., Cordier, P., 2009. Peierls–Nabarro modelling of dislocations in MgO from ambient pressure to 100 GPa. Model. Simul. Mater. Sci. Eng. 17. http://dx.doi.org/10.1088/0965-0393/17/3/035010, 035010-1521.

Cordier, P., Amodeo, J., Carrez, P., 2012. Modelling the rheology of MgO under Earth's mantle pressure, temperature and strain rates. Nature 481, 177–180. http://dx.doi.org/10.1038/nature10687.

Davies, D.R., Goes, S., Davies, J.H., Schuberth, B.S.A., Bunge, H.P., Ritsema, J., 2012. Reconciling dynamic and seismic models of Earth's lower mantle: the dominant role of thermal heterogeneity. Earth Planet. Sci. Lett. 353–354, 253–269. http://dx.doi.org/10.1016/j.epsl.2012.08.016.

Denoual, C., 2004. Dynamic dislocation modeling by combining Peierls Nabarro and Galerkin methods. Phys. Rev. B 70. http://dx.doi.org/10.1103/PhysRevB.70.024106, 024106-1431.

Devincre, B., Kubin, L.P., 1997. Mesoscopic simulations of dislocations and plasticity. Mater. Sci. Eng. A 234, 8–14. http://dx.doi.org/10.1016/S0921-5093(97)00146-9.

Dziewonski, A., Anderson, D., 1981. Preliminary reference Earth model. Phys. Earth Planet. Int. 25, 297–356. http://dx.doi.org/10.1016/0031-9201(81)90046-7.

Girard, J., Chen, J., Raterron, P., 2012. Deformation of periclase single crystals at high pressure and temperature: quantification of the effect of pressure on slip-system activities. J. Appl. Phys. 111, 112607–112615. http://dx.doi.org/10.1063/1.4726200.

Grand, S.P., van der Hilst, R.D., Widiyantoro, S., 1997. Global seismic tomography: a snapshot of convection in the Earth. GSA Today 7, 1–7.

Hager, B.H., 1984. Subducted slabs and the geoid – constraints on mantle rheology and flow. J. Geophys. Res. 89, 6003. http://dx.doi.org/10.1029/JB089iB07p05987.

Hager, B.H., Richards, M.A., 1989. Long-wavelength variations in Earth's geoid: physical models and dynamical implications. Philos. Trans. R. Soc. Lond. A, Math. Phys. Sci. 328, 309–327. http://dx.doi.org/10.1098/rsta.1989.0038.

Houser, C., Masters, G., Shearer, P., Laske, G., 2008. Shear and compressional velocity models of the mantle from cluster analysis of long-period waveforms. Geophys. J. Int. 174, 195–212. http://dx.doi.org/10.1111/j.1365-246X.2008.03763.x.

Kennett, B., Widiyantoro, S., van der Hilst, R.D., 1998. Joint seismic tomography for bulk sound and shear wave speed in the Earth's mantle. J. Geophys. Res. Solid Earth 103, 12469–12493. http://dx.doi.org/10.1029/98JB00150.

Koizumi, H., Kirchner, H., Suzuki, T., 1993. Kink pair nucleation and critical shear stress. Acta Metall. Mater. 41, 3483–3493. http://dx.doi.org/10.1016/0956-7151(93)90228-K.

Kubin, L.P., Devincre, B., Tang, M., 1998. Mesoscopic modelling and simulation of plasticity in fcc and bcc crystals: dislocation intersections and mobility. J. Comput. Aided Mater. Des. 5, 31–54. http://dx.doi.org/10.1023/A:1008648120261.

Kustowski, B., Ekström, G., Dziewoński, A.M., 2008. Anisotropic shear-wave velocity structure of the Earth's mantle: a global model. J. Geophys. Res. 113, B06306. http://dx.doi.org/10.1029/2007JB005169.

Li, C., van der Hilst, R.D., Engdahl, E.R., Burdick, S., 2008. A new global model for P wave speed variations in Earth's mantle. Geochem. Geophys. Geosyst. 9. http://dx.doi.org/10.1029/2007GC001806.

Lithgow Bertelloni, C., Richards, M.A., 1998. The dynamics of Cenozoic and Mesozoic plate motions. Rev. Geophys. 36, 27–78. http://dx.doi.org/10.1029/97RG02282.

Masters, G., Laske, G., Bolton, H., Dziewonski, A., 2000. The relative behavior of shear velocity, bulk sound speed, and compressional velocity in the mantle. In: Implications for Chemical and Thermal Structure, Earth's Deep Interior: Mineral Physics and Tomography From the Atomic to the Global Scale. Geophysical Monograph Series. American Geophysical Union, Washington, DC. http://dx.doi.org/10.1029/GM117p0063.

Mitrovica, J., Forte, A., 2004. A new inference of mantle viscosity based upon joint inversion of convection and glacial isostatic adjustment data. Earth Planet. Sci. Lett. 225, 177–189. http://dx.doi.org/10.1016/j.epsl.2004.06.005.

Montelli, R., Nolet, G., Dahlen, F.A., Masters, G., 2006. A catalogue of deep mantle plumes: new results from finite-frequency tomography. Geochem. Geophys. Geosyst. 7, 1–69. http://dx.doi.org/10.1029/2006GC001248.

Oeser, J., Bunge, H.-P., Mohr, M., 2006. Cluster design in the Earth Sciences – Tethys. In: High Performance Computing and Communications, Proceedings 4208, 31–40.

Panning, M., Romanowicz, B., 2006. A three-dimensional radially anisotropic model of shear velocity in the whole mantle. Geophys. J. Int. 167, 361–379. http://dx.doi.org/10.1111/j.1365-246X.2006.03100.x.

Paulson, A., Zhong, S., Wahr, J., 2007. Inference of mantle viscosity from GRACE and relative sea level data. Geophys. J. Int. 171, 497–508. http://dx.doi.org/10.1111/j.1365-246X.2007.03556.x.

Ricard, Y., Richards, M., Lithgow-Bertelloni, C., Le Stunff, Y., 1993. A geodynamic model of mantle density heterogeneity. J. Geophys. Res. 98, 21895–21909. http://dx.doi.org/10.1029/93JB02216.

Richards, M.A., Engebretson, D.C., 1992. Large-scale mantle convection and the history of subduction. Nature 355, 437–440. http://dx.doi.org/10.1038/355437a0.

Ritsema, J., Deuss, A., van Heijst, H.J., Woodhouse, J.H., 2010. S40RTS: a degree-40 shear-velocity model for the mantle from new Rayleigh wave dispersion, teleseismic traveltime and normal-mode splitting function measurements. Geophys. J. Int. 184, 1223–1236. http://dx.doi.org/10.1111/j.1365-246X.2010.04884.x.

Schaber, K., Bunge, H.P., Schuberth, B.S.A., Malservisi, R., Horbach, A., 2009. Stability of the rotation axis in high-resolution mantle circulation models: weak polar wander despite strong core heating. Geochem. Geophys. Geosyst. 10, Q11W04. http://dx.doi.org/10.1029/2009GC002541.

Schilling, J.G., 1991. Fluxes and excess temperatures of mantle plumes inferred from their interaction with migrating midocean ridges. Nature 352, 397–403. http://dx.doi.org/10.1038/352397a0.

Schuberth, B.S.A., Bunge, H.P., Ritsema, J., 2009a. Tomographic filtering of high-resolution mantle circulation models: can seismic heterogeneity be explained by temperature alone? Geochem. Geophys. Geosyst. 10, Q05W03. http://dx.doi.org/10.1029/2009GC002401.

Schuberth, B.S.A., Bunge, H.P., Steinle-Neumann, G., Moder, C., Oeser, J., 2009b. Thermal versus elastic heterogeneity in high-resolution mantle circulation models with pyrolite composition: high plume excess temperatures in the lowermost mantle. Geochem. Geophys. Geosyst. 10, Q01W01. http://dx.doi.org/10.1029/2008GC002235.

Schuberth, B.S.A., Zaroli, C., Nolet, G., 2012. Synthetic seismograms for a synthetic Earth: long-period P- and S-wave traveltime variations can be explained by temperature alone. Geophys. J. Int. 188, 1393–1412. http://dx.doi.org/10.1111/j.1365-246X.2011.05333.x.

Seton, M., Mueller, R.D., Zahirovic, S., Gaina, C., Torsvik, T.H., Shephard, G., Talsma, A., Gurnis, M., Turner, M., Maus, S., Chandler, M., 2012. Global continental and ocean basin reconstructions since 200 Ma. Earth Sci. Rev. 113, 212–270. http://dx.doi.org/10.1016/j.earscirev.2012.03.002.

Shephard, G.E., Bunge, H.P., Schuberth, B.S.A., Müller, R.D., Talsma, A.S., Moder, C., Landgrebe, T.C.W., 2012. Testing absolute plate reference frames and the implications for the generation of geodynamic mantle heterogeneity structure.

Earth Planet. Sci. Lett. 317–318, 204–217. http://dx.doi.org/10.1016/j.epsl.2011.11.027.

Simmons, N.A., Forte, A.M., Boschi, L., Grand, S.P., 2010. GyPSuM: a joint tomographic model of mantle density and seismic wave speeds. J. Geophys. Res. 115, B12310. http://dx.doi.org/10.1029/2010JB007631.

To, A., Romanowicz, B., Capdeville, Y., Takeuchi, N., 2005. 3D effects of sharp boundaries at the borders of the African and Pacific Superplumes: observation and modeling. Earth Planet. Sci. Lett. 233, 137–153. http://dx.doi.org/10.1016/j.epsl.2005.01.037.

van der Hilst, R.D., Widiyantoro, S., Engdahl, E.R., 1997. Evidence for deep mantle circulation from global tomography. Nature 386, 578–584. http://dx.doi.org/10.1038/386578a0.

Weygand, D., Gumbsch, P., 2005. Study of dislocation reactions and rearrangements under different loading conditions. Mater. Sci. Eng. A 400, 158–161. http://dx.doi.org/10.1016/j.msea.2005.03.102.

Yang, L.H., Söderlind, P., Moriarty, J.A., 2001. Atomistic simulation of pressure-dependent screw dislocation properties in bcc tantalum. Mater. Sci. Eng. A 309–310, 102–107. http://dx.doi.org/10.1016/S0921-5093(00)01618-X.